Layout Synthesis of CMOS MEMS Accelerometers

Vishal Gupta and Tamal Mukherjee
Department of ECE, Carnegie Mellon University, Pittsburgh, PA-15213

Abstract

An optimal layout synthesis methodology for CMOS MEMS accelerometers is presented. It consists of a parametrized layout generator that optimizes design objectives while meeting functional specifications. The behavior of the device is estimated using lumped parameter analytical equations. The design problem is then formulated into a non-linear constrained optimization problem. Such an approach to automated design of MEMS devices helps the designer to explore design trade-offs efficiently. Synthesis of cell level devices is also required for structured design of integrated MEMS. Designs for a CMOS MEMS accelerometer for different optimization objectives, as well as possible design trade-offs are discussed.

Keywords: Synthesis, CAD, CMOS MEMS accelerometer

Introduction

Recently, CMOS micromachining [1] has emerged as a key fabrication technology for VLSI MEMS. The design and characterization of a lateral accelerometer fabricated using CMOS micromachining was first reported in [2]. There is increasing interest towards integrated microsystems, like an inertial measurement unit, which use an array of similar topology devices (like accelerometers and gyroscopes) with different performance specifications for enhanced performance. Such integrated systems necessitate the use of CAD tools to design cell level MEMS devices [3].

The layout synthesis methodology presented here automates the design of CMOS accelerometers for different performance requirements. Extending on a previous synthesis methodology for polysilicon lateral accelerometers [4], the enhancements required to handle multiple routing layers in CMOS micromachining are discussed.

Behavioral specifications, lumped-parameter analytical models and topology-dependent geometrical constraints are used to formulate the design problem into a non-linear constrained optimization (and sizing) problem. Once the layout design parameters are obtained from this optimization, a hierarchical layout generator is used to produce the mask geometries required for the sensor layout. This encoding of human design expertise into a synthesis tool allows the designer to explore a larger design space and to consider system-level trade-offs.

CMOS Accelerometer Description

The CMOS micromachining technology [1] uses a 0.5μ three metal layer CMOS process. After the normal CMOS foundry fabrication, an anisotropic reactive ion etch (RIE) is used to etch away the unmasked oxide layers to define the sidewalls of the microstructure. Finally, an isotropic RIE is performed to etch away the silicon substrate and release the microstructures, as shown in Fig. 1. The top metal layer acts as a mask for both the post-processing steps. This technology allows multiple signal routes within the same mechanical structure. Also, the microstructures are approximately 20 μm above the substrate leading to designs with low parasitic capacitance.

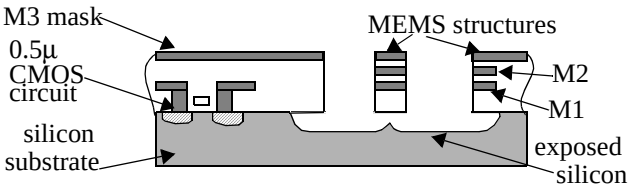

ig. 1: A CMOS-MEMS chip cross-section

The topology of the accelerometer used here is that of a single-axis, common-centroid, fully-differential, capacitive-sensing lateral accelerometer [2, 5]. The schematic is shown in Fig. 2. The proof mass is suspended using four serpentine springs attached to its corners. Interdigitated comb-drives are used for differential capacitive sensing (shown in the schematic), as well as for force feedback balancing (not shown). Each rotor finger consists of two electrical nodes (using multiple routes through the plate-mass), one each for the two capacitors on the half capacitive bridge; and the sense nodes are located on the stator fingers. This is used to create a common-centroid configuration, which is not possible in polysilicon MEMS. In order to counter out-of-plane curl mismatch between the comb-fingers, the stator fingers are attached to a peripheral frame rather than being anchored to the substrate.

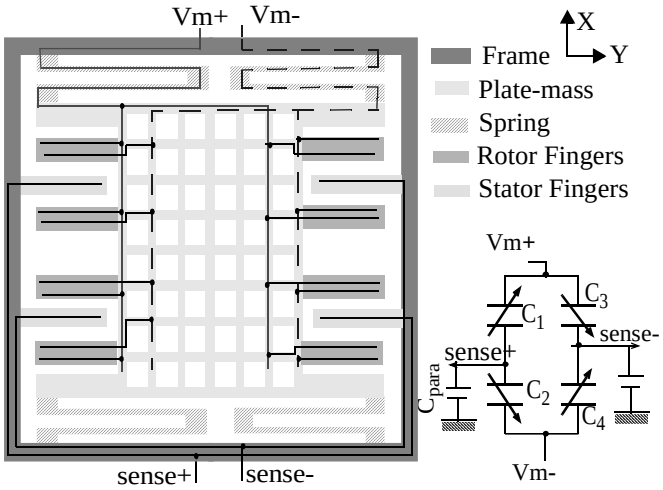

Fig. 2: Accelerometer topology schematic

The accelerometer is modeled as a second order mechanical (mass-spring-damper) system followed by a capacitive transducer. Analytical equations in three modes (in-plane *x, y, and* θ*)* are used to characterize the behavior of the accelerometer. The viscous damping experienced by the accelerometer is modeled as Couette-flow damping below the plate-mass, Stokes-flow above the accelerometer, and squeeze-film damping between the comb-fingers [4]. For this design, squeeze-film damping *usually* dominates over all other forms of damping, requiring more accurate models [6]. The electrical behavior of the accelerometer is modeled as a capacitive bridge with parasitic capacitance, with,

$$V_{sense+} = \frac{2(C_1 - C_2)V_m}{C_1 + C_2 + C_{para}}$$

where V_m is the high frequency modulation voltage applied across the bridge, and C_1, C_2 and C_{para} are as shown in Fig. 2. The parasitic capacitance (C_{para}) consists of the sensor layout parasitic capacitance (computed during synthesis) and the input capacitance of the first gain-stage of the read-out circuit (specified by the user as a lumped quantity). The noise of the system is modeled as Brownian noise of the mechanical system and the user-specified input referred noise of the first gain-stage of the read-out circuit ($\bar{v}_{n\text{-}ckt}$).

$$Total\ Noise = \sqrt{\left(\frac{\overline{v_{n-ckt}}}{Sensitivity}\right)^2 + (\overline{Brownian\ Noise})^2}$$

In order to generate a parametrized layout, all the geometry variables in the layout need to be quantified. The variables which directly affect the device performance (called *design variables*) are varied during optimization to obtain an optimal solution. The main design variables for accelerometer layout synthesis are: length and width of the central plate-mass, sizes and number of beams used in the sepentine spring, number of sensing and feedback fingers, size of electrostatic gap between the combfingers, and the length and width of the rotor fingers. The variables which do not affect the device behavior directly, like the width of stator finger, would always be chosen by the optimization to have some constant value in order to maximize performance. Such variables are called *style variables*, and are fixed to their known optimal values. Additionally, the effect of some variables on device behavior is not completely modeled. Such variables, like the size of anchor, are fixed to values that have worked fine in earlier experiments [2,5].

The next section discusses the synthesis methodology using the constraints defined for the design variables and the behavioral characteristics of the accelerometer.

Layout Synthesis

Plate-mass Design

The plate-mass in a CMOS accelerometer consists of unit squares with etch holes for release. Ideally, the synthesis methodology would like to optimize the size of these squares and mass density. However, this unit square is chosen to have a fixed size since, the exact *non-linear* relationship between the size of etch holes required to release a particular area of plate-mass is not yet determined. Plate-mass with unit squares of this fixed size (9 μm with 6 μm etch hole) has been repeatedly released in earlier experiments. Thus, the design variables for the plate-mass are reduced to: the number of unit squares in *x* and *y* directions.

The plate-mass is defined by M3 layer, which is always grounded. A fixed topology routing network uses M1 and M2 to conduct signals to the rotor fingers, as shown in Fig. 2. The plate-mass area not being used for routing is filled with grounded M1 and M2, all metal layers contributing to increasing the density and lowering the curl in the structure.

Rotor Finger Design

Each rotor finger has two electrical nodes as shown in Fig. 2. For maximum sidewall capacitance, all the layers (poly, M1, M2 and M3) are shorted on each electrical node. Since, two electrical nodes have to be separated on a single mechanical finger, the process design rules for electrical separation define the lower limit on the width of the finger. This width (4 μm for a 0.5μ process) is equally shared by the two electrical nodes. The upper limit on finger-width is determined by the release constraints. The maximum width of finger that can be released with minimum (design-rule correct) gap around it has been experimentally determined to be 5.7 μm.

The upper limit on length of the rotor finger is set by out-of-plane curl limitations, an unavoidable feature of multi-layered structures. Instead of the absolute out-of-plane curl, we are limited by the relative curl in the rotor and stator fingers. Though, the peripheral frame matches the curl between rotor fingers and stator fingers to first order, it does not eliminate the curl mismatch completely. Thus, an experimentally determined limit of 120 μm is set for maximum finger length. For preliminary curl match in the fingers, the stator finger width is fixed to be the lower limit on the rotor finger width. Further investigations to characterize the curl mismatch relationship as a function of finger length in the presence of a frame are underway. Use of this relationship in synthesis will lead to more optimal designs.

Spring Design

The in-plane behavior of the serpentine springs is fully characterized using analytical models mentioned in [7], which are within 5% of FEM simulations. The effect of spring mass on the system behavior is taken into account using effective mass of the spring in *x* and *y* directions (using the static mode shapes). A serpentine spring with odd number of truss beams is used. As shown in [7], such a spring topology has very low cross-axis sensitivity. A very stiff beam is used at each corner to connect the plate-mass to the springs. In order to ensure that this connecting beam does not affect the cross-axis properties of the serpentine spring, a constraint is placed on its stiffness to be higher than ten times the

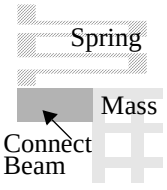

spring stiffness ($K_{x(\text{connect beam})} > 10*K_{x(\text{spring})}$), with the width of this beam used as a design variable.

For reduced lateral curl, the spring beams consist of all three, equally wide metal layers; though least possible metallization in the spring beams would be preferred for more flexibility.

Other Design Constraints

In order to ensure the validity of behavioral equations used, the resonant frequency modes for the major axis (*x*) and the non-major axes (*y* and θ) are constrained to be separated by at least a factor of 2. Similar resonant frequency models have been verified in [4]. For better accuracy, the resonant frequency of each individual rotor finger is also constrained to be separated from the modulation voltage frequency (by a minimum factor of 1.5). The accelerometer design is behaviorally constrained to meet the user specifications of sensitivity, noise, range, cross-axis sensitivity, bandwidth and total sensor area. In addition, there are geometrical constraints that ensure the validity of physical layout, *e.g.*, all the sense and force units have to fit on the plate-mass. Constraints on gaps around different structures are determined from their release characteristics, *e.g.*, the thick connecting beam needs more gap around it as compared to the thin spring beams.

Synthesis Algorithm

Using the design and style variables and the design constraints discussed in previous section, the problem is formulated into a non-linear constrained optimization problem. All equality constraints are eliminated to minimize the number of design variables in the optimization. This optimization (sizing) problem is solved using standard optimization solvers [8]. The search for a solution is guided by an optimization objective, which can be — to minimize area, noise or to maximize sensitivity.

In order to avoid local minima in the cost function, a multi-grid point start algorithm is used [4]. These starting points are determined using a design-of-experiments style approach to partitioning the multivariate design space. In order to handle integer valued variables, a branch-and-bound approach is followed.

After obtaining the design variable values, a hierarchical parametrized layout generator is used to generate the layouts for the constituting elements: spring, comb-finger, plate-mass, routing, and for the complete sensor.

Results and Discussion

A prototype tool has been developed based on the synthesis methodology described in the previous sections. Layouts of CMOS accelerometers synthesized using this tool, for three different optimization objectives, are presented here. A short comparison of the area optimization case with a manual design is also presented. Finally, the sensitivity *vs.* noise trade-off for accelerometer design is discussed.

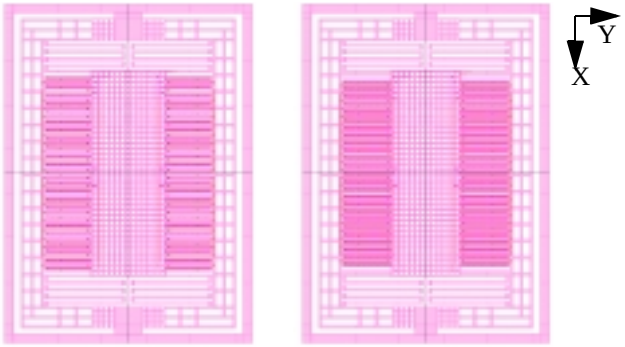

(a) Gap=2.6 μ*m* ω=5.8 kHz (b) Gap=1.5 μ*m* ω=5 kHz

Fig. 3: Accelerometers optimized for (a) minimal noise & (b) maximal sensitivity

Noise and Sensitivity Optimization

The accelerometers presented in Fig. 3 have a common specification of sensitivity 0.5 mV/G, range 50 G, bandwidth 1 kHz, cross-axis sensitivity 1%, noise floor 100 $\mu G/\sqrt{Hz}$, and maximum allowed area of 500 x 270 $(\mu m)^2$. The specified area limits are based on a manual design [5]. Additionally, the circuit noise is specified to be *10 nV/*$\sqrt{Hz}$, and the input capacitance of the circuit to be 230 *f*F.

Synthesis with an objective to minimize noise results in a design shown in Fig. 3(a). The system noise predicted by the synthesis module is *50* $\mu G/\sqrt{Hz}$. This design uses maximum allowed area to capture maximal mass. The highlight of this design is a *large gap between the rotor and stator fingers*. This shows that for the current specifications, squeeze film damping in the finger gaps dominates over other forms of damping, and that the Brownian mechanical noise dominates over electrical noise. Thus, the optimal solution to minimize noise is to enlarge finger gaps, and compensate for the reduced sensitivity with a low resonant frequency.

Fig. 3(b) shows the accelerometer layout optimized for maximal sensitivity under the noise constraint. The highlights of this design are: *a narrow finger gap and a flexible spring*. Both of these design choices lead to increased sensitivity (softer spring ⇒ reduced resonant frequency, narrow finger gap ⇒ increased sense capacitance). Due to limited area, an increase in number of spring beams leads to decrease in plate-mass size, and hence decrease in number of rotor fingers. Thus, the maximum allowed area places a limit on the maximum sensitivity obtainable within a particular amount of noise. For 100 $\mu G/\sqrt{Hz}$ noise, maximal sensitivity of *1.97 mV/G* is obtained.

Area Optimization vs. Manual Design

Fig. 4(a) is our reference, manually designed accelerometer [5] with sensitivity of 0.5 mV/G and noise of 83 $\mu G/\sqrt{Hz}$. The remaining characteristics of this design are same as the specifications for the noise and sensitivity optimizations above. Synthesis for minimizing area with specifications equal to that of the manual design results in the design

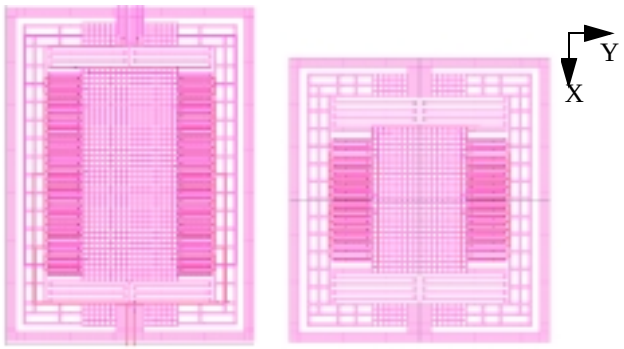

(a) K_x=1.56
Mass=0.56 µg Gap=1.5 µ*m*

(b) K_x=0.63
Mass=0.38 µg Gap=1.65 µ*m*

Fig. 4: (a) Manually designed accelerometer
(b) Accelerometer optimized for minimal area

shown in Fig. 4(b). This design *uses a flexible spring*, so that the sensitivity specification can be met with least possible mass and hence, area. The noise specification places a lower limit on the mass, to counter which the finger-gap is also slightly increased in this optimization. The synthesized accelerometer shows a 21% area improvement over the manual design, and has the maximum allowed noise floor of 83 $\mu G/\sqrt{Hz}$. For experimental verification of the models used in synthesis, prototype synthesized accelerometers are currently under fabrication.

Design Space Exploration

Fig. 5 shows the sensitivity *vs.* noise trade-off in accelerometer design optimization. The designs are optimized to minimize noise for different sensitivity values. The total system noise consists of mechanical Brownian noise and the electrical circuit noise. The minimum noise is obtained at the sensitivity of 0.4 mV/G. The discrete humps in the curves is due to presence of integer valued variables.

Naively, one would think that larger mass ⇒ larger sensitivity and lower noise. But, as shown in Fig. 5, for the given sensor configuration, *the finger-gap dominates the noise figure* rather than the mass. In order to minimize

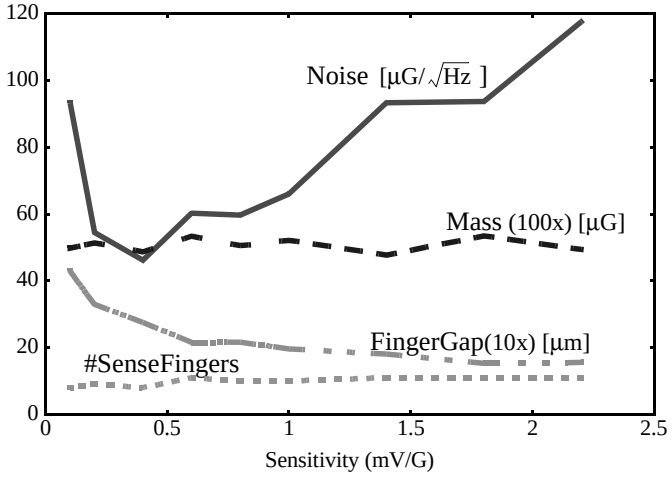

Figure 5: Sensitivity *vs.* Noise trade-off

mechanical noise, optimization tends to maximize the finger-gap (thus, reducing the damping). However, *to the right side of 0.4 mV/G sensitivity, the mechanical noise dominates over electrical noise, while to its left, the electrical noise dominates over mechanical noise*. Consequently, towards the right, higher sensitivity ⇒ lower finger-gap ⇒ higher damping ⇒ higher mechanical noise ⇒ higher system noise. On the other hand, to the left, decreasing sensitivity ⇒ increasing contribution of electrical noise ⇒ increasing system noise despite decreasing mechanical noise.

Coupling the above trade-off analysis with a parasitic capacitance-*vs*.-noise curve (instead of lumped values) for the read-out circuit can lead to an optimal system design.

Conclusions

The design and layout generation of CMOS accelerometers has been successfully automated using a synthesis methodology based on lumped parameter behavioral models. The optimizations performed using a prototype tool suggest significant improvements over manual designs. The trade-off analyses possible with synthesis help understand the design issues from a system level perspective. For example, as shown in the sensitivity *vs.* noise trade-off analysis, if the system is operating in the region towards right of the noise minima, the system will benefit by reducing mechanical noise (by increasing proof-mass); while to the left, the system will benefit more by a lower noise circuit design rather than by a better sensor design. Thus, a systematic approach to synthesis of MEMS devices can lead to an *optimal system design* in addition to optimal sensor design.

Acknowledgments

This research effort is sponsored by the Defense Advanced Research Projects Agency (DARPA), under agreement number F30602-96-2-0304.

References

[1] G. K. Fedder, *et. al.*, "*Laminated high-aspect-ratio structures in a conventional CMOS process*," Sensors & Actuators, A 57, pp. 103-110 (1996).

[2] G. Zhang, *et. al.*, "*A Lateral Capacitive CMOS Accelerometer with Structural Curl Compensation*," IEEE MEMS '99, Orlando.

[3] T. Mukherjee & G. K. Fedder, "*Structured Design of MEMS*," Proc. 97 Design Automation Conference.

[4] T. Mukherjee, *et. al.*, "*Automated Optimal Synthesis of Microaccelerometers*," IEEE MEMS '99, Orlando.

[5] H. Luo, *et. al.*, "*A 1 mG Lateral CMOS-MEMS Accelerometer*," IEEE MEMS '00, Japan.

[6] S. Vemuri, *et. al.*, "*Low-Order Squeeze Film Model for Simulation of MEMS Devices*," MSM 2000, San Diego.

[7] S. Iyer, *et. al.*, "*Analytical Modeling of Cross-axis Coupling in Micromechanical Springs*," MSM '99, Puerto Rico.

[8] P.E. Gill, *et. al.*, "*User's Guide for NPSOL (Version 4.0): A Fortran Package for Nonlinear Programming*," Technical Report SOL 86-2, Stanford University, January 1986.